

Picking, grasping, or scooping small objects lying on flat surfaces: A design approach

The International Journal of
Robotics Research
2018, Vol. 37(12) 1484–1499
© The Author(s) 2018
Article reuse guidelines:
sagepub.com/journals-permissions
DOI: 10.1177/0278364918802346
journals.sagepub.com/home/ijr



Vincent Babin and Clément Gosselin 

Abstract

Grasping in constrained environments is, to this day, an ongoing research topic. Objects can rarely be grasped from arbitrary directions, hence the need to study the options available to grasp them. This paper proposes a gripper capable of grasping small or thin objects that cannot be directly pinch-grasped. The focus is placed on objects that lie on hard surfaces. The proposed approach uses a quasistatic method referred to as scooping while implementing a passive thumb to compensate for manipulator positioning errors. Hence, the robot arm does not need to be moved while the gripper is grasping an object, similarly to a human hand performing a precision grasp. The design approach is presented and the main design choice, namely the use of epicyclic gear trains instead of conventional revolute joints, is explained. The implementation of the proposed approach to the gripper design is shown. We explain how parallel pinch grasps and large grasping forces are achieved even though the mechanism does not follow the usual parallelogram four-bar implementation of parallel pinch mechanisms. The experimental validation of the proposed concept is then presented by picking up a set of test objects in sequence and demonstrating some variants of the method that expand on the concept.

Keywords

Gripper, hand, grasping, manipulation, robot, joint mechanism, epicyclic mechanism, extrinsic dexterity, compliant mechanism, robot finger, robot thumb

1. Introduction

The development of robotic grippers that can pick up or hold a large variety of objects is still an active research topic. When studying the needed capabilities of a gripper, some research works focus on a given set of objects (Borst et al., 2004; Guay et al., 2014), effectively trying to find the best force distribution to maintain these objects in place. In the process of studying the force-object relations, some studies choose to neglect the friction forces of the system, ultimately to come up with more robust solutions. Other studies focus on the very capable human hand to study its behavior and obtain a categorization of the grasps or taxonomies (Cutkosky, 1989; Feix et al., 2016), with the goal of being able to choose simpler grasp primitives for a hand design. In fact, Ceccarelli (2013) states that, according to statistical studies, 60% to 70% of grasps are achieved using only two fingers, which suggests that designs that are much simpler than anthropomorphic hands should be favored.

Regardless of the method employed, an important distinction should be made between studies that simplify the problem by assuming that the object is floating in space (Birglen et al., 2007; Miller et al., 2003) (hence, all faces

are attainable) and those that acknowledge the environment of the object in the form of other objects occluding the workspace or the constraints of the environment itself (e.g. a gripper, a wall, or a table). Studying the environment and the ways to take advantage of it in order to re-position or complete tasks eventually leads to the concept of extrinsic dexterity (Dafle et al., 2014), which involves relying on resources extrinsic to the hand or gripper. Recent studies focus on dealing with the grasping of objects in cluttered environments and solutions are proposed to the trajectory planning problem for an existing gripper (Berenson et al., 2007). A promising research avenue is to take advantage of adjacent features (e.g. a hard surface or table) to perform grasps (Amend et al., 2012; Eppner et al., 2015; Kazemi et al., 2014).

Department of Mechanical Engineering, Université Laval, Canada

Corresponding author:

Clément Gosselin, Department of Mechanical Engineering, Université Laval, Pavillon Adrien-Pouliot, 1065 Avenue de la médecine, Québec, QC, G1V 0A6, Canada.
Email: Clement.Gosselin@gmc.ulaval.ca

Nevertheless, one of the key research issues is the design of the grippers themselves. Depending on the tasks and requirements, a variety of solutions have been proposed in the literature. For example, if it is required to only lift a flat and nonporous object, a simple suction cup can be used (Kessens and Desai, 2011). Other proposed solutions involve the use of microscopic hair-like features to exploit van der Waals forces in order to lift objects, even in the absence of form closure (Hawkes et al., 2016). Other designs feature mechanical fingers activated by electric motors. Some of these designs are very compact, incorporating the motors inside the gripper itself (Odhner et al., 2014; Quigley et al., 2014). Many researchers developed mechanisms with the goal of having fast-closing fingers while also being capable of exerting large forces when needed. This type of behavior is typically obtained through the use of a mechanism that switches mode after contact to passively increase the transmission ratio (Shin et al., 2012; Spanjer et al., 2012; Takaki and Omata, 2011; Takayama et al., 2009). Some of these grippers feature great in-hand manipulation capabilities (Tadakuma et al., 2012), some of them having the ability to obtain form closure by using a great degree of adaptability in the form of reconfigurable hands (Demers and Gosselin, 2011; Quigley et al., 2014; Wei et al., 2011). However, these rigid designs are less adapted for contact with very stiff environments.

A topic explored in recent years is the design of soft grippers that feature the capability to deal with rigid environments with a certain degree of compliance (Catalano et al., 2014; Dollar and Howe, 2007; Odhner et al., 2014). Some of the proposed designs are especially effective in the presence of positioning errors or unforeseen collisions, i.e., they have their fingers bent away to prevent damage (Catalano et al., 2014; Odhner et al., 2014). Solutions to the problem of grasping thin rigid objects lying on hard surfaces were proposed by Babin et al. (2019) and Odhner et al. (2013). In the latter study, a human-inspired grasp and an underactuated gripper interacting with the object and the surface are used while in the former reference, the finger is slid under the objects which are held in place by applying a topside force.

Another important issue in the design of linkage-based grippers is the limited range of motion provided by revolute joints when parallelogram four-bar mechanisms are employed to achieve precision parallel grasps. To alleviate this drawback, some researchers explored the use of planetary or epicyclic mechanisms (Babin et al., 2019; Koganezawa and Ishizuka, 2008). This concept was also used to couple electric motors having different properties in mechanical drives (Babin et al., 2014). When used in finger joints, epicyclic mechanisms also allow the separation of the phalanges, which provides robustness and compact design (Catalano et al., 2014).

Although the design proposed by Catalano et al. (2014) cleverly deals with specific features, an important factor that must be taken into account is not only how the hand moves on its own but how the forces are applied once the

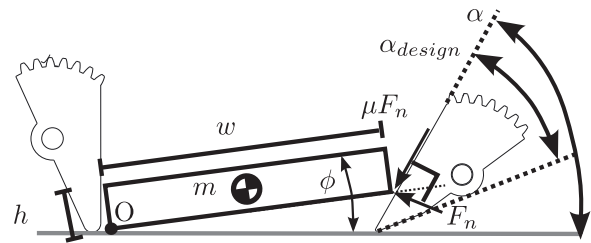


Fig. 1. Planar static model used to study the scooping grasp.

gripper is in contact with the object and the environment (Eppner et al., 2015).

In this context, this work aims to present a proof of concept of a method that solves the problem of picking up objects lying on hard surfaces while simultaneously ensuring contact with the environment in a simple way. The goal is also to incorporate the basic features of standard grippers, such as parallel pinch grasp, self-locking, and the use of conventional electric actuators, in the design while keeping an acceptable size that does not prevent the gripper from accessing cluttered environments.

In this paper, the statics of the scooping grasp are first studied in order to gain insight into this type of grasp and to develop gripper design guidelines. Then, based on these results, a novel gripper design is presented and its kinematic analysis is detailed. The design constraints that guarantee the feasibility of the parallel pinch grasps are shown and the corresponding constraint equations are derived. The force capabilities of the proposed design are also studied. Then, three types of scooping methods are described and analyzed, namely, rigid scooping, compliant scooping, and idle scooping. To clearly demonstrate the effectiveness of the novel gripper concept, a prototype is designed and built and the design parameters are provided. Additionally, some of the design features are discussed, including the thumb mechanism, which allows easy insertion under the objects without having to use sharp fingertips.

2. Static model of the scooping grasp

This section introduces a static model of the scooping grasp, which involves using the distal phalanx of a finger to create an artificial wall on one side of an object while using the distal phalanx of a second finger referred to as the thumb, to slide beneath the object from the opposite side. The representation shown in Figure 1 is used to obtain the free-body diagram of the object. Figure 1 shows that the finger (rounded fingertip on the left) is used to create the aforementioned artificial wall, making the object pivot about point O . It follows that the thumb slides under the object with an attack angle α . The rest of the variables are the object height (h), width (w), and mass (m), the force normal to the thumb surface (F_n), and the friction force (μF_n), assuming friction is proportional to F_n . Angle ϕ represents the orientation of the object with respect to the

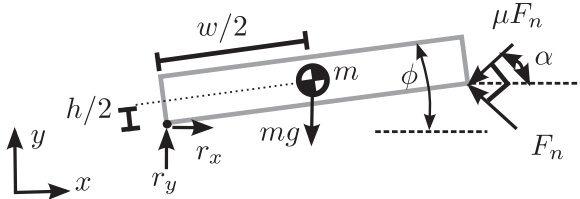


Fig. 2. Free-body diagram of the reaction forces acting on the object.

base surface. It is important to point out that considering the gripper design, α cannot take values smaller than α_{design} , where α_{design} refers to the geometry of the distal phalanx, as shown in Figure 1. The resulting free-body diagram is shown in Figure 2, where g stands for the gravitational acceleration.

Applying the laws of statics, i.e., taking the sum of the moments on the object with respect to point O , on the representation shown in Figure 2, and solving for F_n yields

$$F_n = \frac{mg(\cos \phi - \frac{h}{w} \sin \phi)}{2(\cos(\alpha - \phi) - \mu \sin(\alpha - \phi))} \quad (1)$$

Equation (1) is arranged in order to yield F_n explicitly. Considering that there is a maximum force that can be achieved by the actuators to insert the thumb, minimizing the reaction forces lessens the reliance on powerful motors for a successful insertion. Hence, minimizing the quantity appearing on the right-hand side of equation (1) is then the goal. First, it is assumed that the object parameters m , h , and w are given, since it is desired to focus on design parameters, i.e., object parameters cannot be modified.

We first study the object in its original configuration, i.e., $\phi = 0$. A second assumption is that the objects being picked up are flat and thin, i.e., h/w is very small. Even though the numerator of equation (1) only contains object variables, it is worth mentioning that as the thumb is being inserted under the object, i.e., as ϕ increases, larger values of h/w will make the numerator decrease faster. Hence, picking up the object by the narrowest side will yield better results. In fact when ϕ starts from 0 and increases, the numerator of equation (1) decreases until the object is at an angle $\phi = \tan^{-1}(-h/w) + \pi$, which, for very thin objects, i.e., if $h/w \rightarrow 0$, yields an object angle of $\phi = \pi$ radians. This means that, in all cases considered in this study, the numerator of equation (1) decreases monotonically when ϕ increases. A similar reasoning can be made for the denominator, which decreases until a value of $\phi = \tan^{-1}(-\mu)$ is reached. With a value of $\mu = 0.4$, which corresponds to acrylonitrile butadiene styrene (ABS) resin on steel (Totten, 1992), this value is equal to 111.8° . This result suggests that F_n is a maximum at the initial insertion and decreases monotonically as the thumb is being inserted. Therefore, it is possible to focus on the initial insertion of the thumb, i.e., $\phi = 0$, rather than the whole sliding under the object. Hence, it can be concluded that

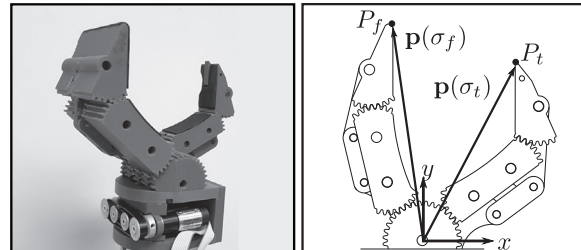


Fig. 3. Side view of the proposed gripper.

orienting the object to yield the largest value of the ratio h/w and designing the gripper so that the friction coefficient between the object and the gripper is as small as possible will yield the best results. Also, the gripper should be designed such that the value of angle α can be minimized to favor the insertion. In other words, it should be ideally possible to flex the finger until $\alpha = \alpha_{\text{design}}$ and α_{design} should be as small as realistically possible.

3. Proposed gripper design

As mentioned, the last phalanx of one of the fingers should be flexed inwards to favor scooping grasps. Therefore, since this brings both fingertips closer together, scooping objects from a flat surface requires a large grip opening and hence a large range of motion for each phalanx relative to the other adjacent phalanges. The range of motion of pin joints, which are typically used in finger design, are here mentioned to have two major drawbacks for the task at hand. The first is that, in practice, for large movement of a revolute joint, it is harder to keep the inner surfaces of the fingers from colliding into each other, hence locking the fingers for large openings. The second is that the mechanism, being a revolute joint, needs all the movement to be provided by the transmission mechanism it is connected to. To alleviate this drawback, epicyclic mechanisms are used here because they allow one to easily select the input-output ratio of a given joint while providing a very large range of motion. Additionally, a two-finger design is selected in this work, mainly because the presented methods are based on planar grasping and because two contact points are sufficient to hold an object in the presence of friction. Following this, each of the two fingers is designed with different properties, as shown in Figure 3. As shown in this figure, the fingers have different width and link lengths, thereby yielding different input-output properties. For ease of notation, the two fingers are referred to as $i = f$ for the finger and $i = t$ for the thumb. Therefore when referring to θ_{1i} , for the thumb, we have θ_{1t} .

Figure 4 shows the finger on the right, which is wider than the thumb shown on the left. This choice was made so that one of the fingers has a large contact area, enabling it to better distribute pressure when supporting heavy objects.

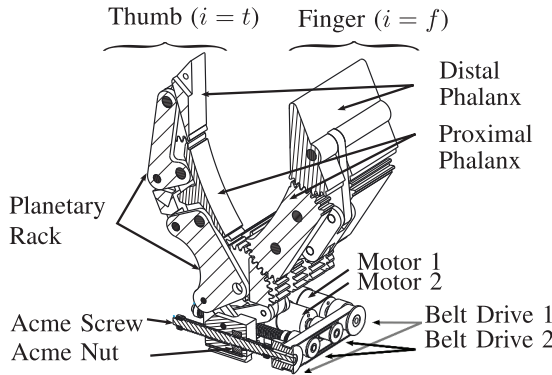


Fig. 4. Cut view of the proposed gripper.

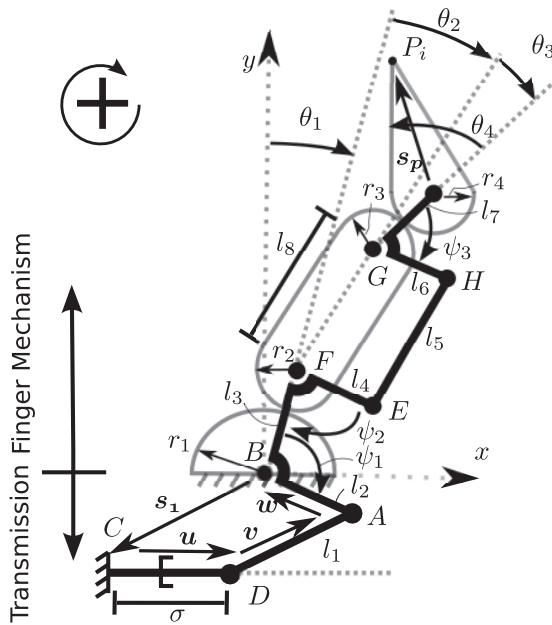


Fig. 5. Kinematic model of the finger and transmission.

Each of the fingers is driven by a slider crank mechanism which in turn is driven by a belt drive. A slider crank mechanism is used because it can provide a large force amplification when needed. Each belt drive consists of a motor on one end driving an acme screw. The two belt drives are assembled so that the belts are concentric for compactness. The mechanism is studied in two parts, namely the finger mechanism and the transmission mechanism, as shown in Figure 5.

3.1. Epicyclic mechanism kinematics

A kinematic model of the proposed fingers is first established. The two fingers being mirror mechanisms of each other, both are studied in this section according to the diagram shown in Figure 5, which illustrates the geared joints and links constituting the fingers. As opposed to most robot

fingers found in the literature,¹ the proposed design relies heavily on the use of epicyclic mechanisms to achieve large ranges of motion of the joints, yielding the ability to grasp large objects. Using the same notation used in Babin et al. (2014), where the input of the epicyclic mechanism is the carrier and its output is the satellite gear, the mechanism shown in Figure 6 is obtained. Indeed, Figure 6 illustrates the equivalence between the kinematics of the finger and that of a planetary mechanism. The kinematic model of the finger can be described using the following parameters, namely

$$n_1 = \frac{r_1}{r_1 + 2r_2} \quad (2)$$

$$R_1 = \frac{2n_1}{1 - n_1} \quad (3)$$

$$n_2 = \frac{r_3}{r_3 + 2r_4} \quad (4)$$

$$R_2 = \frac{2n_2}{1 - n_2} \quad (5)$$

and hence the kinematic equations describing the motion of the phalanges can be written as

$$\theta_2 = R_1 \theta_1 + \theta_{d1} \quad (6)$$

and

$$\theta_4 = R_2 \theta_3 + \theta_{d2} \quad (7)$$

where r_1 and r_2 are, respectively, the pitch radius of the sun gear and satellite of the base planetary mechanism, r_3 and r_4 (see Figure 5) are, respectively, the pitch radius of the sun gear and satellite of the upper planetary mechanism gear, and, finally, θ_{d1} and θ_{d2} are offset parameters, which are dependent on the initial assembly of the epicyclic mechanisms. Configuration-dependent angles θ_1 , θ_2 , θ_3 , and θ_4 are defined in Figure 5.

3.2. Parallel pinch mechanism

One feature of a two-finger gripper that is generally considered very important in the literature is its ability to keep its distal phalanges parallel to each other in order to perform parallel pinch grasps. Some designs simply use extra actuation to control each phalanx individually. This is, however, more costly in terms of actuation and actually not needed, since passive solutions exist. Cam mechanisms in combination with linkages have been used to allow the parallel pinch grasp (Bartholet, 1992). Other designs use simple four-bar mechanisms to achieve parallel pinch grasps in underactuated hands (Laliberté et al., 2002). Their implementation is shown in Figure 7(a), while the adaptation of this approach to a finger using epicyclic mechanisms is shown in Figure 7(b). Referring to Figure 5, the mechanism consists of the parallelogram $FEHG$ comprising the links

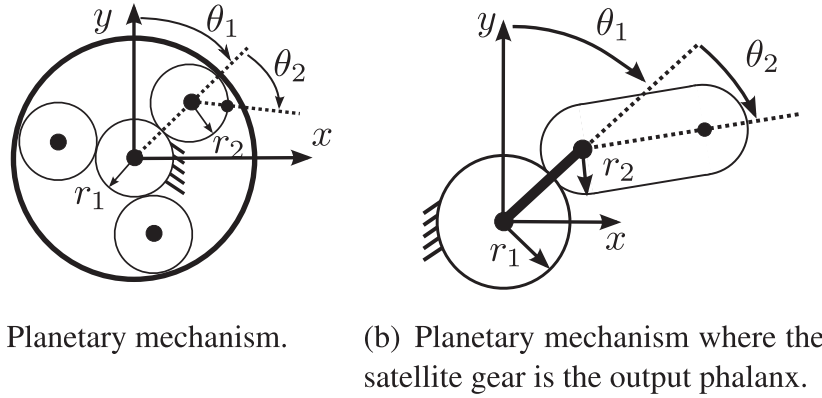


Fig. 6. Generic planetary mechanism and its implementation in the gripper proposed in this paper.

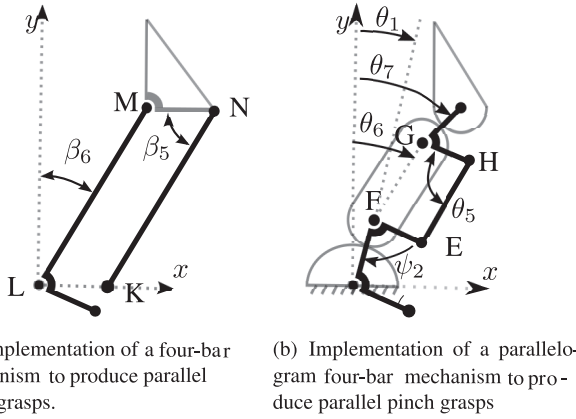


Fig. 7. Two architectures using a four-bar mechanism.

of length ℓ_4 , ℓ_5 , ℓ_6 , and ℓ_8 . To have the four-bar mechanism behave as a parallelogram, the constraints

$$\ell_5 = \ell_8 \quad (8)$$

$$\ell_4 = \ell_6 \quad (9)$$

are imposed.

To better explain the advantages of using four-bar mechanisms combined with the planetary joint mechanisms, the kinematics of the finger mechanism are further developed. First, referring to Figure 5, the following kinematic closure equations are readily obtained

$$\theta_1 + \theta_2 + \theta_3 + \theta_4 = 0 \quad (10)$$

$$\theta_2 + \theta_3 + \psi_2 + \psi_3 = \pi \quad (11)$$

where ψ_2 and ψ_3 are constant design parameters. Secondly, the transmission ratio R_2 (defined in equation (5)) that is required in order to achieve parallel pinch grasps must then be determined. Differentiating equations (10), (11), (6), and (7) yields

$$d\theta_1 + d\theta_2 + d\theta_3 + d\theta_4 = 0 \quad (12)$$

$$d\theta_2 + d\theta_3 = 0 \quad (13)$$

$$d\theta_2 = R_2 d\theta_1 \quad (14)$$

$$d\theta_4 = R_2 d\theta_3 \quad (15)$$

Combining equations (12) through (15), one gets

$$R_1 R_2 = 1 \quad (16)$$

which is the constraint necessary for the distal phalanx to keep a constant orientation relative to the base of the gripper. This result can be expressed as a function of the needed upper planetary pitch diameters by first combining equations (5) and (16) to obtain

$$R_1 \frac{2n_2}{1 - n_2} = 1 \quad (17)$$

Then, using equation (4) to express equation (17) in terms of the pitch radius yields

$$2R_1 \frac{r_3}{r_3 + 2r_4} = 1 - \frac{r_3}{r_3 + 2r_4} \quad (18)$$

which can be rearranged to obtain

$$r_4 = R_1 r_3 \quad (19)$$

Equation (19) is the final condition to be satisfied for the distal phalanx to have a constant orientation with respect to the base throughout the whole range of motion of the finger.

3.3. Transmission angle of the proposed mechanism

Figure 7(a) shows a common implementation of the parallelogram mechanism. Angle β_5 is defined as the transmission angle. Assuming that the input link is the link connecting points L and M , and that the output link is the link connecting points M and N , then angle β_5 must deviate as little as possible from 90° in order to obtain the proper force transmission properties of the four-bar linkage. Expressing the transmission angle as a function of the input angle θ_6 , one gets

$$\beta_5 = \frac{\pi}{2} - \beta_6 \quad (20)$$

By inspection of Figure 7(b), we get

$$\pi = \psi_2 + \theta_5 + \theta_6 - \theta_1 \quad (21)$$

and from Figure 6(b), Figure 7(b), and equation (6), we can write

$$\theta_6 = (R_1 + 1)\theta_1 + \theta_{d1} \quad (22)$$

which we can solve for θ_1 and substitute into equation (21) to get the expression of θ_5 as function of θ_6 , yielding

$$\theta_5 = \pi - \psi_2 - \frac{\theta_{d1}}{R_1 + 1} - \frac{R_1}{R_1 + 1}\theta_6 \quad (23)$$

where θ_{d1} is a constant mechanical design parameter. To study the force transmission capabilities, we differentiate equations (20) and (23), which yields

$$d\beta_5 = -d\beta_6 \quad (24)$$

$$d\theta_5 = -\frac{R_1}{R_1 + 1} d\theta_6 \quad (25)$$

By inspection of equations (24) and (25), it can be observed that the deviation of the transmission angle can be adjusted in the proposed mechanism by selecting parameter R_1 , whereas it is fixed in the case of the mechanism shown in Figure 7(a).

3.4. Finger kinematics

Referring to Figure 5, vector \mathbf{p} is defined as the position vector of the tip of the finger (point P_i) with respect to the origin of the fixed frame (point B). Using angles

$$\theta_6 = \theta_1 + \theta_2 \quad (26)$$

$$\theta_7 = \theta_1 + \theta_2 + \theta_3 \quad (27)$$

shown in Figure 7(b), vector \mathbf{p} can then be expressed as

$$\mathbf{p} = \begin{bmatrix} l_3 \sin \theta_1 + l_8 \sin \theta_6 + l_7 \sin \theta_7 \\ l_3 \cos \theta_1 + l_8 \cos \theta_6 + l_7 \cos \theta_7 \end{bmatrix} + \mathbf{s}_p \quad (28)$$

where \mathbf{s}_p is the vector shown in Figure 5 pointing from the pivot of the distal phalanx to the fingertip. Combining equations (27) and (11), angle θ_7 can be expressed as a function of θ_1 , as

$$\theta_7 = \theta_1 + \pi - \psi_2 - \psi_3 \quad (29)$$

Differentiating equation (28) with respect to time, using equation (6), and noting $s_1 = \sin \theta_1$, $c_1 = \cos \theta_1$, $s_6 = \sin \theta_6$, $c_6 = \cos \theta_6$, $s_7 = \sin \theta_7$, and $c_7 = \cos \theta_7$ then yields

$$\dot{\mathbf{p}} = \begin{bmatrix} l_3 c_1 + (R_1 + 1)l_8 c_6 + l_7 c_7 \\ -l_3 s_1 - (R_1 + 1)l_8 s_6 - l_7 s_7 \end{bmatrix} \dot{\theta}_1 \quad (30)$$

which provides the velocity of the fingertip as a function of the input velocity $\dot{\theta}_1$.

3.5. Transmission mechanism

The fingers are independent from each other and have separate transmission mechanisms. Each finger uses a lead-screw mechanism as a linear actuator, which in turn drives a slider crank mechanism, as shown in Figure 5. To find the relationship between the input and output of the transmission mechanism, the following vector-loop equation is first written

$$-\mathbf{v} = \mathbf{s}_1 + \mathbf{u} + \mathbf{w} \quad (31)$$

where the vectors are defined in Figure 5. Vector \mathbf{s}_1 is a constant vector, $\mathbf{u} = \sigma_i [1 \ 0]^T$, $\mathbf{w} = l_2 [-\sin(\theta_1 + \psi_1) - \cos(\theta_1 + \psi_1)]^T$, $\mathbf{v}^T \mathbf{v} = l_1^2$, and σ_i the actuator input coordinate, as shown in Figure 5. Taking the square of the norm of each side of equation (31) yields

$$\mathbf{v}^T \mathbf{v} = (\mathbf{s}_1 + \mathbf{u} + \mathbf{w})^T (\mathbf{s}_1 + \mathbf{u} + \mathbf{w}) = l_1^2 \quad (32)$$

which can be expanded as

$$2(\mathbf{s}_1 + \mathbf{u})^T \mathbf{w} + (\mathbf{s}_1 + \mathbf{u})^T (\mathbf{s}_1 + \mathbf{u}) + l_2^2 - l_1^2 = 0 \quad (33)$$

Using $A_k = -2l_2(\mathbf{s}_1 + \mathbf{u})^T \mathbf{e}_1$, $B_k = -2l_2(\mathbf{s}_1 + \mathbf{u})^T \mathbf{e}_2$, and $C_k = (\mathbf{s}_1 + \mathbf{u})^T (\mathbf{s}_1 + \mathbf{u}) + l_2^2 - l_1^2$, equation (33) can be rearranged as

$$A_k \sin(\theta_1 + \psi_1) + B_k \cos(\theta_1 + \psi_1) + C_k = 0 \quad (34)$$

where $\mathbf{e}_1 = [1 \ 0]^T$, $\mathbf{e}_2 = [0 \ 1]^T$, and $k = t, f$ (thumb and finger). Equation (34) can be solved for θ_1 as a function of the input σ_i , as

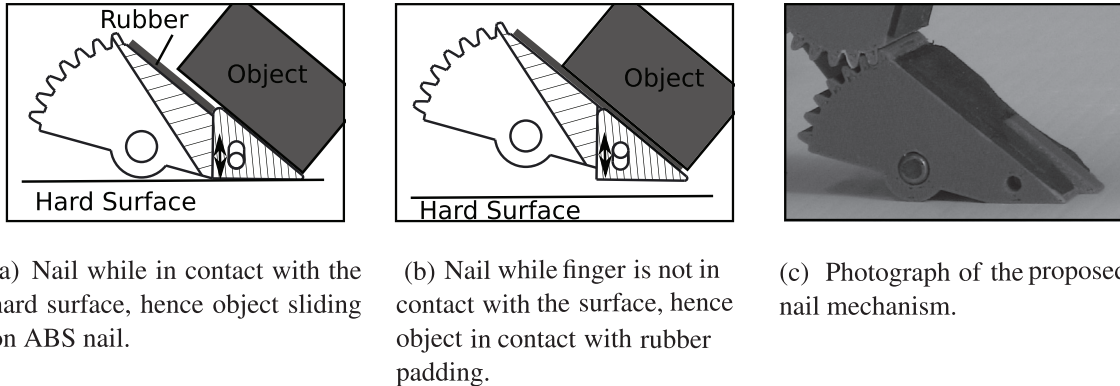


Fig. 8. Side cut view of the nail mechanism in use and when retracted, and photograph of the prototype.

Table 1. Geometric parameters of prototype.

Parameter	Thumb (mm)	Finger (mm)
l_1	17.27	21.59
l_2	26.67	18.79
l_3	41.14	41.14
l_4	17.78	13.97
l_5	27.94	27.94
l_6	17.78	13.97
l_7	41.14	41.14
l_8	27.94	27.94
r_1	22.60	22.60
r_2	18.54	18.54
r_3	18.54	18.54
r_4	22.60	22.60
σ_{\max}	25.40	22.86
s_1	$[-0.76 \quad -25.40]^T$	$[-17.01 \quad -25.40]^T$
s_p	$[-14.22 \quad 26.92]^T$	$[-14.22 \quad 24.89]^T$
Parameter	Thumb (degrees)	Finger (degrees)
ψ_1	85	110
ψ_2	100	120
ψ_3	105	85
θ_{d1}	-55	-55
θ_{d2}	0	0
$\theta_{3\min}$	-40.65	—
α_{design}	38.66	—

$$\theta_1 = 2 \tan^{-1} \left(\frac{-A_k - \sqrt{A_k^2 - B_k^2 - C_k^2}}{C_k - B_k} \right) - \psi_1 \quad (35)$$

Once angle θ_1 has been computed, all other angles are readily obtained using equations (22) and (29).

3.6. Retractable nail

Following the reasoning presented in Section 2, based on equation (1), a material as slippery as possible against all materials should be used as the coating for the inside of the

thumb. However, this is detrimental to the ability of the gripper to hold on to objects once grasped. Indeed, the surface of the fingers should have the highest coefficient of friction possible to prevent the object from slipping away when held.

To resolve these conflicting design objectives, a retractable nail feature, shown in Figure 8, is used to enhance the scooping procedure while still taking advantage of the high friction coefficient of rubber or other similar padding against objects when grasped. Taking advantage of the contact with the surface, the nail protrudes through the thumb; this allows the object to slide on it during the scooping motion, as shown in Figure 8(a). Once the object is being lifted from the surface or once the back of the phalanx is no longer in contact with the surface, the nail is pushed back through the thumb and the object makes contact with the high-friction surface of the phalanx, thereby providing a high friction coefficient, as shown in Figure 8(b).

4. Properties of the gripper

A prototype of the gripper was designed and built. Most of the components were 3D printed and are made of ABS plastic. To elaborate on the capabilities of the gripper, the prototype's geometric parameters, which satisfy the constraints to achieve precision pinch grasps (equations (10) and (11)), are shown in Table 1. Parameter $\theta_{3\min}$ is only given for the thumb because it is a study parameter used in an upcoming section of the paper and not a design parameter.

The capabilities of the gripper are demonstrated by studying two grasping procedures. The first, referred to in this paper as lock-gripping, refers to the ability of the gripper to exert very large forces on an object for a certain range of object width. The second behavior, the study of which forms the main contribution of this paper, is a procedure referred to here as scooping, where the finger of the gripper creates a wall while the thumb slides under the object in a scooping manner in order to grasp thin objects lying on hard surfaces.

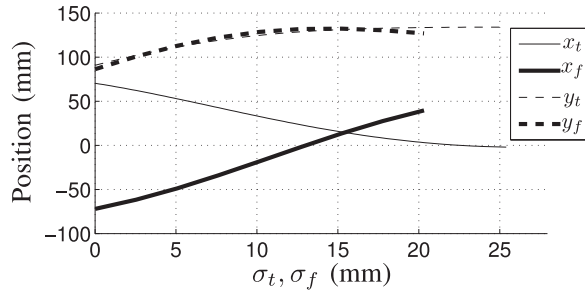


Fig. 9. Position of the tip of the thumb (x_t, y_t) and of the finger (x_f, y_f), respectively, as a function of the thumb linear actuator coordinate σ_t and the finger linear actuator coordinate σ_f .

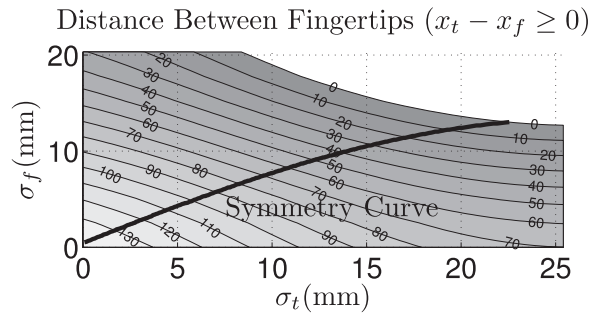


Fig. 10. Distance between the tip of the thumb and the tip of the finger along the x -axis as a function of the thumb linear actuator coordinate σ_t and the finger linear actuator coordinate σ_f .

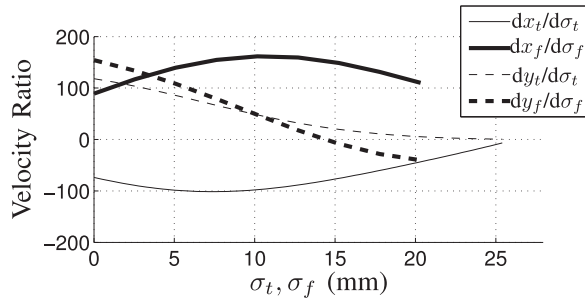


Fig. 11. Velocity ratios of the tip of the thumb (\dot{x}_t, \dot{y}_t) and of the finger (\dot{x}_f, \dot{y}_f) over the input velocity ($\dot{\sigma}_t$ and $\dot{\sigma}_f$) as a function of the position of the thumb linear actuator σ_t and the position of the finger linear actuator coordinate σ_f .

5. Grasping with large forces (lock-gripping)

To study the force characteristics of the gripping process, the kinematic equations from Section 3 are used. The x and y coordinates of the finger tip and the thumb tip, respectively noted (x_f, y_f) and (x_t, y_t) , are plotted in Figure 9 as a function of the input position of the corresponding actuator. It is recalled that the finger is mirroring the thumb and hence, when using equation (28) to plot the positions of the finger's tip, the negative value

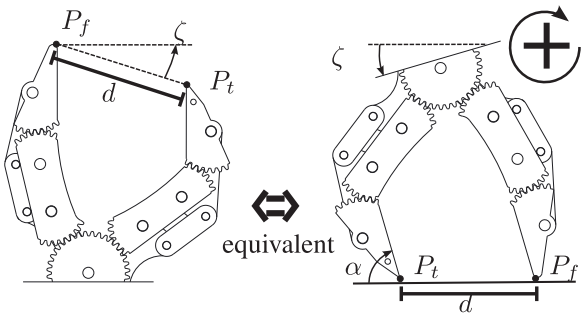
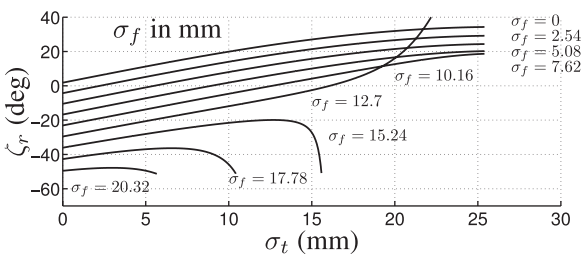
of the x coordinate is used. Since the fingers are undergoing planar motion, the distance between the fingertips along the x -axis is used to determine the width of the objects that can be grasped. To this end, the distance between the fingertips is plotted in Figure 10 as a function of the input coordinates of the fingers using a contour plot in order to show that there are many possible combinations of the two inputs that yield the same object width. In addition, the curve labeled "symmetry curve" represents the unique solution for which the two fingers are at an equal distance from the center of the gripper, i.e., each finger is closing at the same rate with respect to the x -axis.

Analyzing the graph shown in Figure 9, we focus our attention on the zones where the derivative of the position coordinates with respect to the input coordinates is small or equal to zero. Three such zones can be found, namely, x_t and y_t toward the end of their closing trajectory (when σ_t goes to 25.4 mm) and y_f around $\sigma_f = 15.24$ mm. The latter case is of no interest because, using the principle of virtual work, it can easily be shown that, unless a force is acting purely along the y -axis of the gripper, the input-output force ratio is still low, owing to having a low ratio in the x direction. However, the first two zones are interesting because the ratio increases substantially along all axes. To better illustrate this behavior, the derivatives of the tip positions for the thumb and the finger are plotted in Figure 11 using equation (30). It can be observed, in Figure 11, that the derivatives corresponding to the thumb—which are, in fact, components of the Jacobian matrix—both go to zero when σ for each finger goes to its maximum value. Having both fingers independent from each other grants us the ability to apply very large forces on objects by adjusting the finger to the width of the objects and having the final pressure applied by the thumb. The range of object width within which this locking behavior is possible is characterized by the distance between the fingers when the thumb input is at its maximum value. Hence, from Figures 9 and 11, it can be inferred that with the design parameters used here, this locking behavior is possible for object widths ranging from 0 mm to 70 mm (half the gripping range). In summary, large forces can be applied because the finger is self-locking and the thumb is in a special configuration where it can apply large forces.

It should be pointed out that the capability to apply the large forces described here does not compromise the agility (speed) of the gripper, since the large force ratio corresponds only to the end of the range of motion of the thumb. Also, the capability to apply large forces does not represent a safety hazard for compliant objects (such as human fingers, for instance) since the large forces are applied over a very limited range of motion, which yields small deformations of compliant objects for which the grasping forces would remain low. However, for rigid objects, the capability

Table 2. Parameters used to study scooping methods.

Variable	Description
σ_i	Input of i , where i can be “t” for thumb or “f” for finger
ζ_i	Orientation of wrist when using i scooping method, where i can be “r” for rigid, “c” for compliant, or “idle” for idle scooping
α_i	Attack angle of thumb when using i scooping method, where i can be “r” for rigid, “c” for compliant, or “idle” for idle scooping
ζ_{\min}	Optimization parameter used to obtain ζ_c .
ζ_{rot}	Maximum acceptable angle of wrist at which passive thumb can still be activated.
ζ_{opt}	Initial angle of wrist at which attack angle α_c is optimal or minimal.

**Fig. 12.** Equivalent representation to study ζ_r .**Fig. 13.** Gripper orientation ζ_r as a function of the thumb input σ_t for different values of finger input σ_f .

to apply large forces can be very useful in order to secure firm grasps.

6. Scooping

The main contribution of this paper is presented in this section, which considers the task of picking up thin objects resting on a hard surface using three proposed methods, namely, rigid scooping, compliant scooping, and idle scooping. The rigid scooping method aims at presenting a

solution that is easy to understand and visualize but is less robust. The compliant angle scooping introduces compliance in the thumb of the gripper and by design proves to be a highly successful and repeatable method. However, it is rather complicated to implement. Finally, in the idle scooping method, the properties of the gripper mechanism are exploited to find the condition for which the scooping can be performed without the manipulator moving, hence greatly simplifying the implementation of scooping and providing possible near-optimal performances. A lookup table with most of the variables used in the following section and a short list and description of the variables is provided in Table 2.

6.1. Rigid scooping

In this section, we analyze what is required of the manipulator in order to perform the scooping motion. For easier representation of the motions, all movements studied are assumed to take place in the x - y plane. Angle ζ is defined as the angle between a line parallel to the base of the gripper and the line connecting the tip of the finger and the thumb, as shown in Figure 12. Similarly, angle α is defined as the angle between the line connecting the tip of the fingers and the contact surface of the distal phalanx, as shown in Figure 12. In this section, variables ζ_r and α_r refer to ζ and α in the context where the two distal phalanges are parallel to each other. In other words, one degree of freedom per finger is used, as opposed to what is presented in the upcoming sections of this paper, where an extra degree of freedom will be introduced in the thumb.

Figure 12 shows that studying the angle ζ_r formed by the two points P_f and P_t and the horizontal axis is equivalent to considering the wrist angle needed to keep both fingertip tips in contact with the surface. It is pointed out that in this paper, clockwise angles are positive, hence in Figure 12 angle ζ_r is negative and α_r is positive. As explained previously with Figure 11, the design of the gripper combines a faster weaker finger with a stronger slower thumb. As a consequence, if a constant pressure is applied by the fingers on the surface, should the force be high, the mechanism of the finger will be self-locked. Because of this, we study the mechanism so that the position of the finger (σ_f) is kept constant during scooping motions and only the thumb input (σ_t) is driven. Angle ζ_r is plotted in Figure 13 as a function of σ_t for different values of σ_f . Now that we have the plots of the wrist requirements ζ_r , the relation for the attack angle α_r can be written as

$$\alpha_r = \zeta_r + \frac{\pi}{2} \quad (36)$$

which is simply an offset of the curves of Figure 13. However, in order to pick up an object it is also necessary

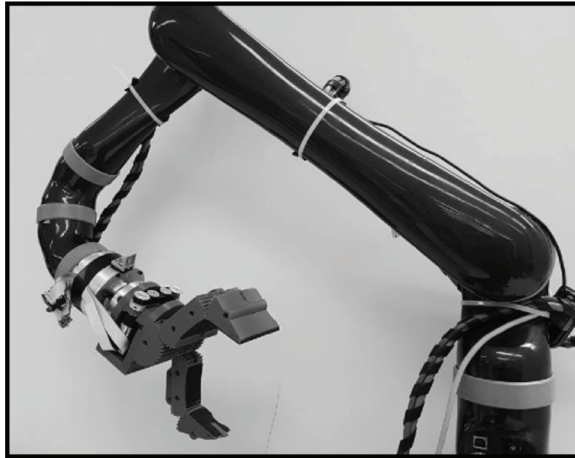


Fig. 14. Prototype of the gripper mounted on a six-degrees-of-freedom manipulator.

to know the distance between the fingertips to verify whether the object initially fits between the fingertips. This distance, here referred to as d_r , represents the object length w , (see Figure 1), that fits between the fingertips. The proposed gripper design is mounted on a six-degree-of-freedom manipulator, as shown in Figure 14 (see also Extension 1) and a rigid scooping sequence is shown in Figure 15 (Extension 2).

It can be observed from Figure 13 and equation (36) that for a wide opening of the gripper, i.e., σ_t and σ_f near zero, the attack angle α_r is close to 90° , hence making it very difficult for the thumb to slide under any object.

In addition to the planning that is required to achieve the rigid maneuver described, hardware issues and potential problems arise before rigid scooping can be achieved. One of the main challenges in this procedure is that of positioning inaccuracies of the fingertips due to positioning errors of both the manipulator and the gripper. For practical applications, very accurate positioning is hard to achieve for all points along the trajectories, hence the contact for both fingertips cannot be ensured in general. A solution to this problem can be to use force sensing to ensure at least one contact with the surface. However, both fingertip contacts would require great model accuracy; this goes against the goal of this paper, which is to provide simple-to-use procedures for the proposed gripper.

6.2. Compliant scooping

In this section, we propose an additional mechanism that introduces a degree of freedom in the thumb in order to enable the manipulator to rely on a single force-sensing device to ensure contact of both fingertips. The advantage that this mechanism provides is that if the fingertip is in contact with the surface, the mechanism guarantees that the tip of the thumb will contact the surface, hence avoiding failure of the grasp due to positioning inaccuracies.

The solution proposed is the modification presented in Figure 16, where the bar linking points H and E in Figure 5 is replaced by a spring with minimal length ℓ_5 . This is achieved by separating the original link into two parts and using an elastic ring to hold the two parts together, hence making the distal phalanx a compliant mechanism. The compliant mechanism allows the distal phalanx to move, relative to the proximal phalanx, under the action of external forces, independently of the thumb input σ_t . This mechanism introduces a new degree of freedom in the gripper; hence the independent variable θ_{3t} is used to fully define the gripper state, i.e., the gripper coordinates are now σ_b , σ_f , and θ_{3t} .

To explain the advantages of the proposed mechanism, we define the quantities ζ_c and ζ_{\min} , shown in Figure 17. The compliant mechanism, when under no external forces, has the thumb behave exactly like in the previous subsection. When under the influence of external forces, the thumb may move over a certain range of motion defined by

$$\theta_{3\min} \leq \theta_{3t} \leq \pi - \psi_2 - \psi_3 - \theta_2 \quad (37)$$

which arises from the two mechanical limits of keeping the gear in mesh and respecting the unstretched distance between points E and H . The variables ζ_c and ζ_{\min} —respectively, the wrist orientation when using the compliant thumb mechanism and the angle between the back of the thumb and the flat surface—are used to determine the orientation that corresponds to the maximum compliance. Further rotation, beyond this orientation, would push parts of the gripper through the surface, assuming that the finger is in contact with the surface.

Furthermore, the following minimization problem

$$\min_{\theta_{3t}} (\zeta_c - \zeta_{\min})^2 \quad (38)$$

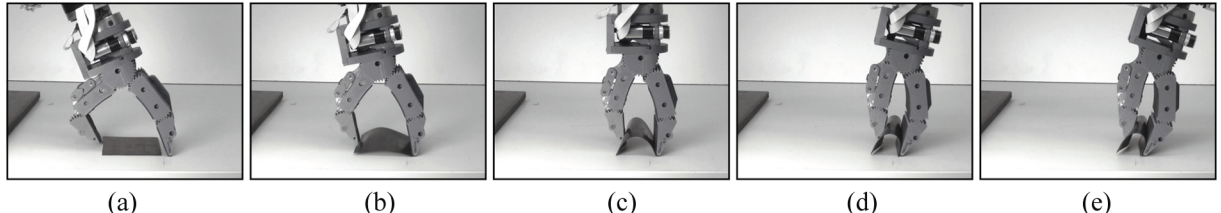


Fig. 15. Rigid scooping example performed with $\sigma_f = 10.16$ mm (see Extension 2).

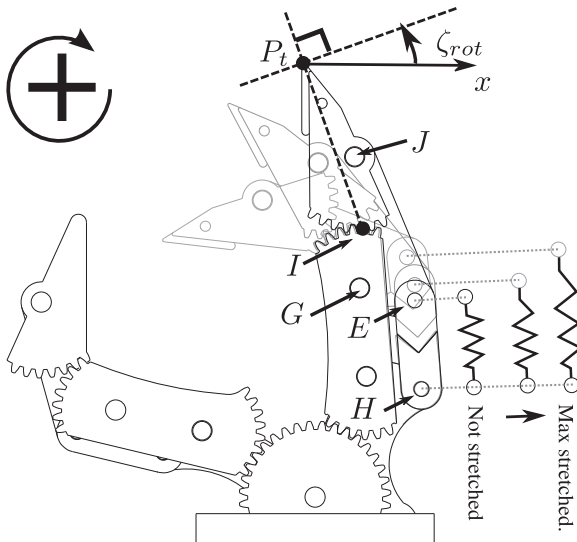


Fig. 16. Unstretched, intermediate, and stretched position of the compliant distal phalanx mechanism. Also shown for the unstretched configuration is the axis connecting the tip of the thumb P_t and the instantaneous center of rotation of the distal phalanx I .

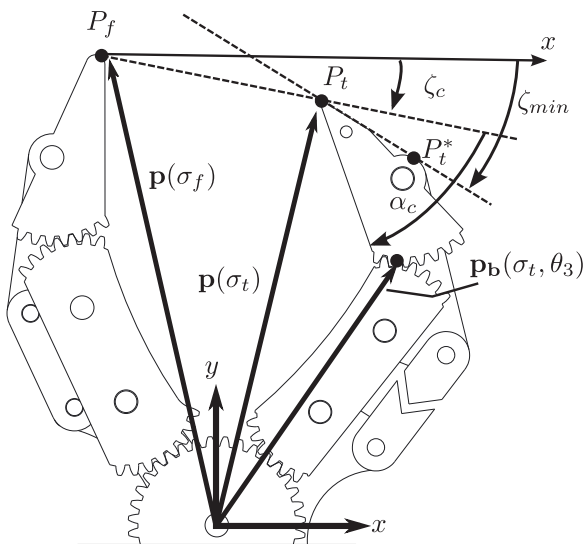


Fig. 17. Parameters used for studying the compliant thumb mechanism.

subjected to the inequality constraints of equation (37) yields the smallest value of ζ_c and consequently the best attack angle α_c . A consequence of the minimization is the relation

$$\zeta_c \leq \zeta_r \quad (39)$$

which states that, for a given σ_f , the rigid scooping orientations will either be less than or equal to the compliant scooping orientation angle for any σ_t . Angles ζ_c and α_c , as well as distance d_c are plotted in Figures 18, 19, and 20 as a function of the thumb input σ_t for the different values of

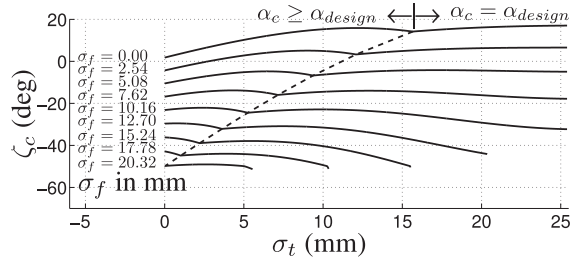


Fig. 18. Manipulator orientation ζ_c , defined as the orientation when the minimal feasible attack angle is achieved, as a function of σ_t for different values of finger input σ_f .

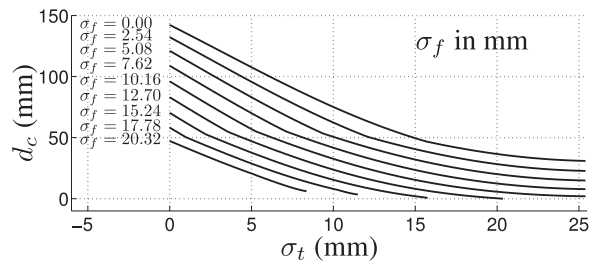


Fig. 19. Manipulator tip-to-tip distance d_c when the minimal feasible attack angle is achieved as a function of thumb input σ_t for different values of finger input σ_f .

the finger input σ_f . The graphs provide a detailed assessment of the properties of the gripper.

An interesting result of this optimization described is that once α_c reduces to a value of α_{design} , it remains constant for the rest of the thumb closing, effectively being at an optimal attack angle, which is possible for the rest of the thumb closing. Figure 21 (see also Extension 3) shows the trajectory of ζ_c for $\sigma_f = 10.16$ mm. As opposed to the rigid scooping shown in Figure 15, it can be observed that here the thumb is correctly inserted under the object.

To determine the condition under which the compliant mechanism is activated, we define in Figure 16 the instantaneous center of rotation of the distal phalanx. Since the distal phalanx is rolling on the proximal phalanx, owing to the use of an epicyclic mechanism, the instantaneous center of rotation is at their meshing point, i.e., point I in Figure 16. Vector \mathbf{p}_b is shown in Figure 17 and is defined as a function of σ_t and θ_{3t} , as

$$\mathbf{p}_b(\sigma_t, \theta_{3t}) = \begin{bmatrix} l_3 \sin \theta_1 + l_8 \sin \theta_6 + r_3 \sin \theta_7 \\ l_3 \cos \theta_1 + l_8 \cos \theta_6 + r_3 \cos \theta_7 \end{bmatrix} \quad (40)$$

Also, angle ζ_{rot} is defined in Figure 16 as the angle between the x -axis and a line perpendicular to the line through points I and P_t . Assuming that there is no friction between the surface and the tip of the thumb, the reaction force is perpendicular to the surface, hence defining ζ_{rot} to give the orientation of the gripper at which the force from the surface will be along the $I-P_t$ axis. Therefore, if the

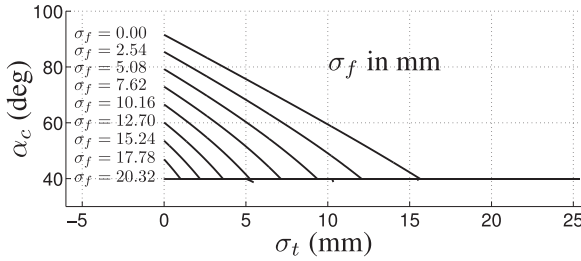


Fig. 20. Minimal achievable attack angle as a function of thumb input σ_t for different values of finger input σ_f .

gripper orientation angle is smaller than ζ_{rot} , approaching the surface perpendicularly activates the compliant mechanism.

To sum up the last two sections, we plot in Figure 22 the values of ζ_r , ζ_c , ζ_{rot} , and ζ_{opt} , which is the angle at which $\alpha_c = \alpha_{\text{design}}$. This figure shows, for various finger actuator positions σ_f , the values ζ_r and ζ_c that, respectively, give the maximum and minimum orientation of the robot wrist for which both fingertips are in contact with the surface, with constant force being applied toward the surface.

6.3. Idle scooping

So far, this paper has focused on the conditions for which fingertip contact can be ensured when executing either rigid or compliant scooping. The rigid form of scooping, while easy to understand and study, was shown to be nonoptimal in terms of the attack angle α that it provided. This led to the study of compliant scooping, which ensures the thumb tip contact but also requires either very precise position control to keep the fingertip at the proper position or force-sensing apparatus to apply pressure on the surface, inherently ensuring fingertip contact.

This subsection outlines a method of performing the scooping procedure at a constant gripper orientation and position. This procedure is therefore very easy to implement, since the robot does not need to move during the scooping action. It is important to notice that the region contained between ζ_r and ζ_c is the range of gripper orientations that ensure contact of the thumb tip when the fingertip is in contact with the surface. To achieve this constant

orientation and position scooping method, referred to as idle scooping, it is required to find a constant orientation value ζ_{idle} , which satisfies

$$\zeta_c \leq \zeta_{\text{idle}} \leq \zeta_r \quad (41)$$

Such values can be found using the plots of ζ_r and ζ_c shown in Figure 22 for a given σ_f , since the finger is assumed locked. The problem amounts to finding horizontal lines in Figure 22 for which equation (41) is valid. In Figure 23, ζ_r and ζ_c are plotted and one possible solution of ζ_{idle} is shown, which is the minimal orientation angle that intersects the curve of ζ_c at its maximum point. This orientation physically represents the gripper orientation for which, once the thumb touches the surface as it closes, the compliant mechanism ensures tip contact with the surface and the angle α is optimal at least once along the trajectory. Figure 24 (see also Extension 4) shows the idle scooping procedure characterized by ζ_{idle} of Figure 23. This method only requires the pose of the end-effector to be in the workspace of the manipulator and the fingertip to be either in contact with the surface or low enough to prevent the object from slipping between the finger and the surface.

Looking at the plots of Figure 23, it can be observed that finding a constant angle scooping orientation ζ_{idle} only involves finding a horizontal line that satisfies equation (41), which corresponds to the shaded zone shown in Figure 23. This behavior is interesting because it does not require any motion of the manipulator during the scooping procedure, and hence does not require precise path following. An example of idle scooping of a coin is shown in Figure 25.

7. Discussion

So far, we focused on explaining the mechanics of the gripper and then proposed three versions of the main contribution of this paper, which is a scooping strategy for grasping thin objects. Here, we discuss scenarios for which the scooping strategies are useful.

As mentioned in the preceding sections, the rigid scooping method, while easy to understand, is not as robust as the other approaches, owing to its heavy reliance on precise trajectories of the manipulator and gripper fingers and its non-optimal thumb insertion angle α .

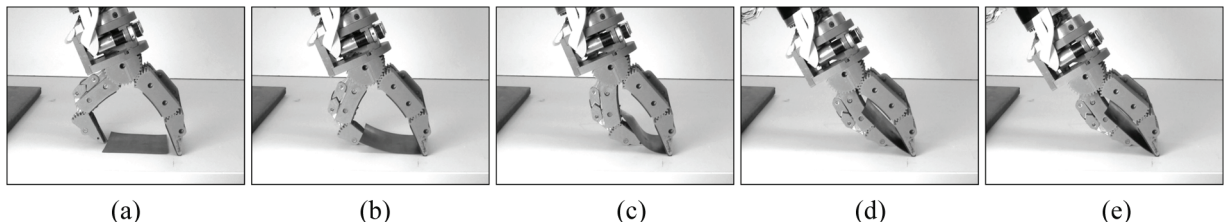


Fig. 21. Compliant scooping example for $\sigma_f = 10.16$ mm (see Extension 3).

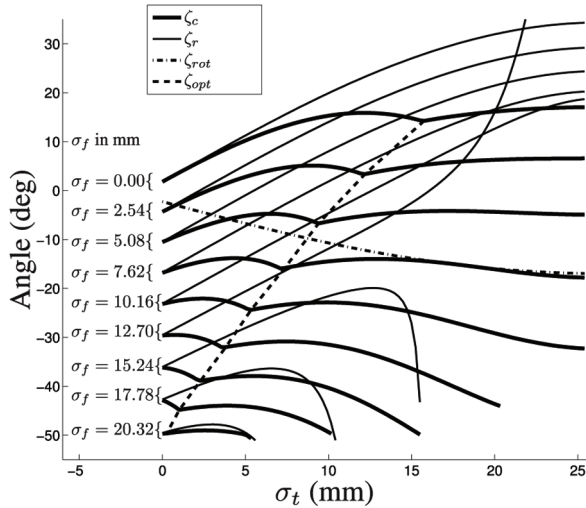


Fig. 22. ζ_r , ζ_c , ζ_{rot} , and ζ_{opt} as a function of the thumb input σ_t for different values of finger input σ_f .

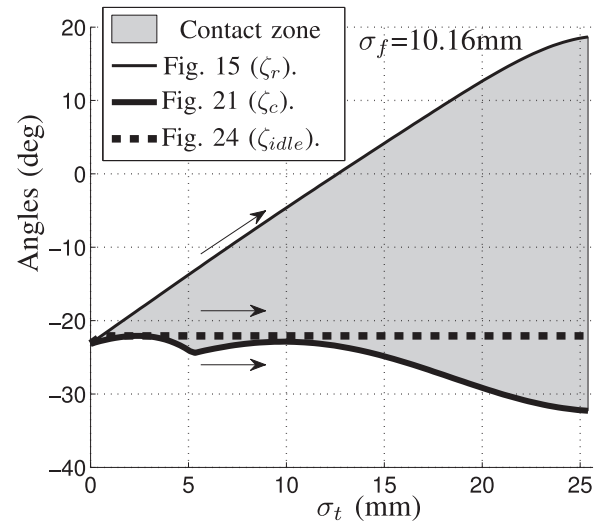


Fig. 23. Required wrist orientations for the trajectories implemented in Figures 15, 21, and 24.

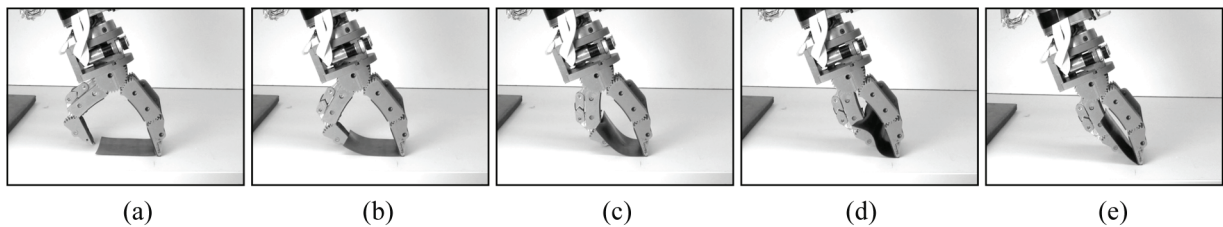


Fig. 24. Example of the constant orientation procedure (idle scooping) for $\sigma_f = 10.16$ mm (see Extension 4).

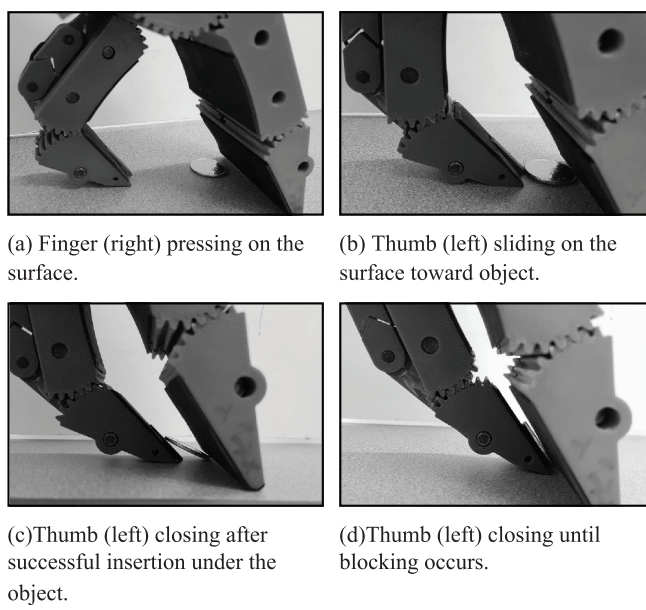


Fig. 25. Idle scooping sequence performed to pick up a thin object, in this case a coin (a quarter).

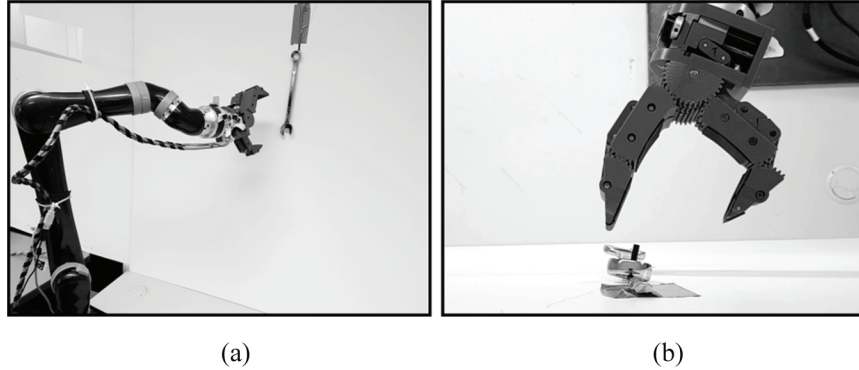


Fig. 26. Proposed constant orientation method (idle scooping) applied on an open-ended wrench hanging from a wall. (a) Robot approaching the hanging wrench. (b) Top view of the gripper before wall contact. The procedure is shown in Extension 5.

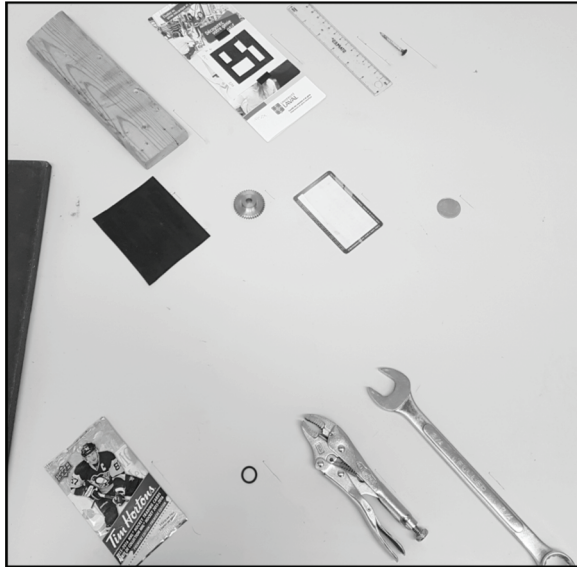


Fig. 27. Set of objects that can be picked up using the proposed idle scooping method (demonstrated in Extension 6). From left to right and top to bottom: wood block, paper pamphlet, plastic ruler, wood screw, thin rubber sheet, metal worm gear, plastic bus card, Canadian quarter, hockey cards pack, o-ring seal, locking pliers, open-ended wrench.

The introduction of the compliant scooping method allowed the use of force sensing to validate fingertip contact with the surface and a range of orientations guaranteeing the thumb tip contact, leaving the user only to follow an orientation strategy. This required force-sensing equipment and corresponding control strategies, in order to maintain contact with the surface. In some cases, force sensing is present in manipulators in the form of an estimate of the error at the manipulator joints. This can sometimes lead to imprecise force measurements in parts of the workspace, depending on the manipulator. A solution can be to add force-sensing devices between the manipulator and the gripper, hence yielding measurements that are independent of the manipulator pose.

The last solution consists of a version of the scooping method that relies solely on bringing the gripper to a target pose and maintaining it. This last method, while not optimal in terms of the attack angle α , can be applied for near-optimal attack angles. This means that, since the orientation is kept constant, it can be implemented by a robot with fewer than six degrees of freedom. For instance, a SCARA robot could have a gripper mounted at a required angle and simply approach the object, lower the gripper until contact and perform the idle scooping method.

Since the idle scooping method does not require manipulator movement while scooping occurs, only the initial contact must be validated in order to perform it. This means that the force-sensing methods used in the application of pressure on the surface can now be simplified to lowering the gripper until a force of a certain magnitude is measured, triggering the manipulator to hold its pose. This suggests that simpler sensing devices can be used to validate this contact, for example a limit switch mounted on the tip of the finger could validate contact and the scooping method is then guaranteed to be successful. The idle scooping method, while so far considered for objects resting on a surface, is not limited to that orientation. An example of the range of application of the method is shown in Figure 26, where the scooping method is performed on an open-ended wrench hanging on a wall (see Extension 5).

To demonstrate the robustness of the idle scooping method, a variety of objects were selected and are shown in Figure 27. In Extension 6, the idle scooping method is performed on all these objects, where the force sensing is only used to detect the contact, i.e., when the magnitude of the force along the z-axis is greater than a given threshold, for example 5 N. All objects are picked up and released in a bin in a single video take to show the robustness of the method.

8. Conclusion

In this paper, a novel gripper design was presented and the kinematics were derived to better understand its function. A

less than effective rigid scooping method was presented in order to understand a simple version of the main contribution of the paper. To easily and simply perform the scooping method, an extra compliant degree of freedom in the thumb was proposed and an optimal trajectory for the manipulator was shown for many configurations of the gripper. Finally, an idle scooping method was presented that not only ensures contact of the thumb tip with the surface but also allows the use of only contact validation sensing to grasp thin objects lying on a flat surface, in addition to allowing the grasping task to be performed with a constant pose of the manipulator.

One aspect that is not covered in this paper is the robustness of the grasping process. Indeed, it has been assumed in this paper that if the object fits within the grasp and if the nail is sharp enough, the grasp will be successful. Future work will focus on incorporating the force capabilities of an arbitrary gripper to further the design guidelines and study the robustness of the method and gripper to positioning inaccuracies of both the robot and the objects, imperfections of the objects, and impact of the properties of the objects.

Funding

This work was supported by the Natural Sciences and Engineering Research Council of Canada, by Prompt Québec and by Robotiq.

ORCID iD

Clément Gosselin  <https://orcid.org/0000-0001-7422-4515>

Note

1. There exist a few finger designs making use of epicyclic mechanisms, as in Catalano et al. (2014).

References

- Amend JR, Brown E, Rodenberg N, et al. (2012) A positive pressure universal gripper based on the jamming of granular material. *IEEE Transactions on Robotics* 28(2): 341–350.
- Babin V, Gosselin C and Allan JF (2014) A dual-motor robot joint mechanism with epicyclic gear train. In: *2014 IEEE/RSJ international conference on intelligent robots and systems*, Chicago, IL, USA, 14–18 September 2014, pp. 472–477. Piscataway, NJ: IEEE.
- Babin V, St-Onge D and Gosselin C (2019) Stable and repeatable grasping of flat objects on hard surfaces using passive and epicyclic mechanisms. *Robotics and Computer-Integrated Manufacturing* 55: 1–10.
- Bartholet S (1992) *Reconfigurable end effector*. Patent 5,108,140, USA.
- Berenson D, Diankov R, Nishiwaki K, et al. (2007) Grasp planning in complex scenes. In: *7th IEEE-RAS international conference on humanoid robots*, Pittsburgh, PA, USA, 29 November–1 December 2007, pp. 42–48. Piscataway, NJ: IEEE.
- Birglen L, Laliberté T and Gosselin CM (2007) *Underactuated robotic hands*. Berlin: Springer.
- Borst C, Fischer M and Hirzinger G (2004) Grasp planning: How to choose a suitable task wrench space. In: *IEEE international conference on robotics and automation, ICRA '04*, New Orleans, LA, USA, 26 April–1 May 2004, vol. 1, pp. 319–325. Piscataway, NJ: IEEE.
- Catalano MG, Grioli G, Farnioli E, et al. (2014) Adaptive synergies for the design and control of the Pisa/IIT softhand. *The International Journal of Robotics Research* 33(5): 768–782.
- Ceccarelli M (2013) *Mechanisms and machine science*. Singapore: Springer.
- Cutkosky MR (1989) On grasp choice, grasp models, and the design of hands for manufacturing tasks. *IEEE Transactions on Robotics and Automation* 5(3): 269–279.
- Dafle NC, Rodriguez A, Paolini R, et al. (2014) Extrinsic dexterity: In-hand manipulation with external forces. In: *IEEE international conference on robotics and automation (ICRA)*, Hong Kong, China, 31 May–7 June 2014, pp. 1578–1585. Piscataway, NJ: IEEE.
- Demers LAA and Gosselin C (2011) Kinematic design of a planar and spherical mechanism for the abduction of the fingers of an anthropomorphic robotic hand. In: *IEEE international conference on robotics and automation*, Shanghai, China, 9–13 May 2011, pp. 5350–5356. Piscataway, NJ: IEEE.
- Dollar AM and Howe RD (2007) Simple, robust autonomous grasping in unstructured environments. In: *IEEE international conference on robotics and automation*, Rome, Italy, 10–14 April 2007, pp. 4693–4700. Piscataway, NJ: IEEE.
- Eppner C, Deimel R, Alvarez-Ruiz J, et al. (2015) Exploitation of environmental constraints in human and robotic grasping. *The International Journal of Robotics Research* 34(7): 1021–1038.
- Feix T, Romero J, Schmidtmayer HB, et al. (2016) The grasp taxonomy of human grasp types. *IEEE Transactions on Human-Machine Systems* 46(1): 66–77.
- Guay F, Cardou P, Cruz-Ruiz AL, et al. (2014) Measuring how well a structure supports varying external wrenches. In: Petuya V, Pinto C and Lovasz EC (eds.) *New advances in mechanisms, transmissions and applications*. Dordrecht: Springer, pp. 385–392.
- Hawkes EW, Jiang H and Cutkosky MR (2016) Three-dimensional dynamic surface grasping with dry adhesion. *The International Journal of Robotics Research* 35(8): 943–958.
- Kazemi M, Valois JS, Bagnell JA, et al. (2014) Human-inspired force compliant grasping primitives. *Autonomous Robots* 37(2): 209–225.
- Kessens CC and Desai JP (2011) A self-sealing suction cup array for grasping. *Journal of Mechanisms and Robotics* 3(4): 045001.
- Koganezawa K and Ishizuka Y (2008) Novel mechanism of artificial finger using double planetary gear system. In: *IEEE/RSJ international conference on intelligent robots and systems*, Nice, France, 22–26 September 2008, pp. 3184–3191. Piscataway, NJ: IEEE.
- Laliberté T, Birglen L and Gosselin C (2002) Underactuation in robotic grasping hands. *Machine Intelligence & Robotic Control* 4(3): 1–11.
- Miller AT, Knoop S, Christensen HI, et al. (2003) Automatic grasp planning using shape primitives. In: *IEEE international conference on robotics and automation*, Taipei, Taiwan, 14–19 September 2003, vol. 2, pp. 1824–1829. Piscataway, NJ: IEEE.
- Odhner LU, Jentoft LP, Claffee MR, et al. (2014) A compliant, underactuated hand for robust manipulation. *The International Journal of Robotics Research* 33(5): 736–752.

- Odhner LU, Ma RR and Dollar AM (2013) Open-loop precision grasping with underactuated hands inspired by a human manipulation strategy. *IEEE Transactions on Automation Science and Engineering* 10(3): 625–633.
- Quigley M, Salisbury C, Ng AY, et al. (2014) Mechatronic design of an integrated robotic hand. *The International Journal of Robotics Research* 33(5): 706–720.
- Shin YJ, Lee HJ, Kim KS, et al. (2012) A robot finger design using a dual-mode twisting mechanism to achieve high-speed motion and large grasping force. *IEEE Transactions on Robotics* 28(6): 1398–1405.
- Spanjer SA, Balasubramanian R, Herder JL, et al. (2012) Improved grasp robustness through variable transmission ratios in underactuated fingers. In: *IEEE/RSJ international conference on intelligent robots and systems*, Vilamoura, Portugal, 7–12 October 2012, pp. 2289–2294. Piscataway, NJ: IEEE.
- Tadakuma K, Tadakuma R, Higashimori M, et al. (2012) Robotic finger mechanism equipped omnidirectional driving roller with two active rotational axes. In: *IEEE international conference on robotics and automation*, Saint Paul, MN, USA, 14–18 May 2012, pp. 3523–3524. Piscataway, NJ: IEEE.
- Takaki T and Omata T (2011) High-performance anthropomorphic robot hand with grasping-force-magnification mechanism. *IEEE/ASME Transactions on Mechatronics* 16(3): 583–591.
- Takayama T, Chiba Y and Omata T (2009) Tokyo-TECH 100 N hand: Three-fingered eight-DOF hand with a force-magnification mechanism. In: *IEEE international conference on robotics and automation*, Kobe, Japan, 12–17 May 2009, pp. 593–598. Piscataway, NJ: IEEE.
- GE Totten (ed.) (1992) *ASM handbook: Friction, lubrication, and wear technology*, vol. 18. Materials Park, OH: ASM International.
- Wei G, Aminzadeh V and Dai JS (2011) Prehension analysis and manipulability of an anthropomorphic metamorphic hand with a reconfigurable palm. In: *IEEE international conference on robotics and biomimetics*, Phuket, Thailand, 7–11 December 2011, pp. 1116–1121. Piscataway, NJ: IEEE.

Appendix: Index to multimedia extensions

Archives of IJRR multimedia extensions published prior to 2014 can be found at <http://www.ijrr.org>, after 2014 all videos are available on the IJRR YouTube channel at <http://www.youtube.com/user/ijrrmultimedia>

Table of multimedia extensions

Extension	Media type	Description
1	Video	Experimental setup and finger range of motion
2	Video	Rigid scooping details and demonstration
3	Video	Compliant scooping details and demonstration
4	Video	Idle scooping demonstration
5	Video	Vertical idle scooping demonstration
6	Video	Multiple objects idle scooping demonstration